

## Quantitative dynamic $^{18}\text{F}$ FDG-PET and tracer kinetic analysis of soft tissue sarcomas

Espen Rusten, Jan Rødal, Mona E. Revheim, Arne Skretting, Øyvind S. Bruland & Eirik Malinen

To cite this article: Espen Rusten, Jan Rødal, Mona E. Revheim, Arne Skretting, Øyvind S. Bruland & Eirik Malinen (2013) Quantitative dynamic  $^{18}\text{F}$ FDG-PET and tracer kinetic analysis of soft tissue sarcomas, Acta Oncologica, 52:6, 1160-1167, DOI: [10.3109/0284186X.2012.728713](https://doi.org/10.3109/0284186X.2012.728713)

To link to this article: <https://doi.org/10.3109/0284186X.2012.728713>



Published online: 03 Dec 2012.



Submit your article to this journal [↗](#)



Article views: 1101



View related articles [↗](#)



Citing articles: 5 View citing articles [↗](#)

## ORIGINAL ARTICLE

**Quantitative dynamic  $^{18}\text{F}$ FDG-PET and tracer kinetic analysis of soft tissue sarcomas**ESPEN RUSTEN<sup>1</sup>, JAN RØDAL<sup>1</sup>, MONA E. REVHEIM<sup>2</sup>, ARNE SKRETTING<sup>2</sup>, ØYVIND S. BRULAND<sup>3,4</sup> & EIRIK MALINEN<sup>1,5</sup>

<sup>1</sup>Department of Medical Physics, The Norwegian Radium Hospital, Oslo University Hospital, Oslo, Norway, <sup>2</sup>Department of Radiology and Nuclear Medicine, The Norwegian Radium Hospital, Oslo University Hospital, Oslo, Norway, <sup>3</sup>Department of Oncology, The Norwegian Radium Hospital, Oslo University Hospital, Oslo, Norway, <sup>4</sup>Faculty of Medicine, University of Oslo, Oslo, Norway and <sup>5</sup>Department of Physics, University of Oslo, Oslo, Norway

**Abstract**

**Purpose.** To study soft tissue sarcomas using dynamic positron emission tomography (PET) with the glucose analog tracer [ $^{18}\text{F}$ ]fluoro-2-deoxy-D-glucose ( $^{18}\text{F}$ FDG), to investigate correlations between derived PET image parameters and clinical characteristics, and to discuss implications of dynamic PET acquisition (D-PET). **Material and methods.** D-PET images of 11 patients with soft tissue sarcomas were analyzed voxel-by-voxel using a compartment tracer kinetic model providing estimates of transfer rates between the vascular, non-metabolized, and metabolized compartments. Furthermore, standard uptake values (SUVs) in the early (2 min p.i.;  $\text{SUV}_E$ ) and late (45 min p.i.;  $\text{SUV}_L$ ) phases of the PET acquisition were obtained. The derived transfer rates  $K_1$ ,  $k_2$  and  $k_3$ , along with the metabolic rate of  $^{18}\text{F}$ FDG ( $\text{MR}_{\text{FDG}}$ ) and the vascular fraction  $v_p$ , was fused with the computed tomography (CT) images for visual interpretation. Correlations between D-PET imaging parameters and clinical parameters, i.e. tumor size, grade and clinical status, were calculated with a significance level of 0.05. **Results.** The temporal uptake pattern of  $^{18}\text{F}$ FDG in the tumor varied considerably from patient to patient.  $\text{SUV}_E$  peak was higher than  $\text{SUV}_L$  peak for four patients. The images of the rate constants showed a systematic pattern, often with elevated intensity in the tumors compared to surrounding tissue. Significant correlations were found between  $\text{SUV}_{E/L}$  and some of the rate parameters. **Conclusions.** Dynamic  $^{18}\text{F}$ FDG-PET may provide additional valuable information on soft tissue sarcomas not obtainable from conventional  $^{18}\text{F}$ FDG-PET. The prognostic role of dynamic imaging should be investigated.

Sarcomas are heterogeneous tumors with a low incidence rate (~1%) and a high number of histological subtypes (~50). High grade soft tissue sarcomas may be treated with surgery, chemotherapy, and radiotherapy [1]. Due to the heterogeneity of sarcomas it is desirable to identify physiological attributes such as vasculature and metabolism describing tumor biology and malignancy potential.

[ $^{18}\text{F}$ ]fluoro-2-deoxy-D-glucose positron emission tomography ( $^{18}\text{F}$ FDG PET) may visualize the abnormal glycolytic metabolism of cancer cells non-invasively. There is an ongoing evaluation of the use of PET images to predict and evaluate therapeutic response for personalized treatment of sarcoma [2,3]. However, the lack of standardization of research

studies limits available cases and the role of  $^{18}\text{F}$ FDG PET in diagnosis and staging of sarcomas is still unclear [4].

Conventional, static  $^{18}\text{F}$ FDG PET gives a single snapshot image typically acquired one hour after injection. This PET image mostly reflects metabolism. However, the  $^{18}\text{F}$ FDG concentration in tissue depends on the vascular supply, and residual, free (non-metabolized)  $^{18}\text{F}$ FDG in the blood and tissue is also of importance. Dynamic PET (D-PET) can be used to compensate for these confounding effects by analyzing a complete sequence of images acquired from the time of  $^{18}\text{F}$ FDG injection. Furthermore, surrogate maps of tissue vascularization may potentially be derived from D-PET [5,6]. Traditionally, images

of tissue vascularization have been obtained with dynamic contrast-enhanced (DCE) imaging, either by computed tomography (CT) or magnetic resonance imaging (MRI). As solid tumors require neovascularization to maintain growth, such images may complement the metabolic information obtained from conventional  $^{18}\text{F}$ FDG PET.

In tracer kinetic analysis of D-PET image sequences, the time-concentration characteristics are analyzed in terms of a physiological model. The model parameters may represent biological features of the tissue in question, and are thus attractive in cancer phenotyping. D-PET, together with tracer kinetic analysis, has been used to estimate tissue vascularization as well as metabolism to improve the predictions of cancer therapy response [7]. It has further been proposed that altered blood flow and hypoxia may indicate regions selecting for more aggressive tumor strands and radiation resistance [8]. Hence, the additional vascular information obtained may be relevant for biological image-guided radiation therapy [9,10]. Furthermore, in the event that both a PET scan and a DCE scan is requested, D-PET represents an alternative single examination producing both vascular and metabolic information. D-PET may thus save the patient from one examination and the injection of contrast agent, reducing the risk of contrast-induced nephropathy.

In the present study, image parameters from  $^{18}\text{F}$ FDG D-PET scans of 11 patients with high grade soft tissue sarcoma were evaluated. A two-compartment model was utilized to calculate pharmacokinetic parameters as measures of vasculature and tumor cell metabolism [11–13]. Parameter maps were calculated, uptake dynamics were described, and correlations between PET derived parameters and clinical characteristics were investigated.

## Material and methods

### Patients

The study comprised 11 patients with high grade (III or IV) soft tissue sarcomas (Table I). Five patients had tumors in the torso, four had tumors in the legs and two had tumors in the hip region. The women had a median age of 76 years (range 42–81 years) and median weight 80 kg (range 62–124 kg). The men had a median age of 53 years (range 37–66 years) and a median weight of 84 kg (range 65–95 kg). Seven patients underwent surgery with post operative radiation therapy and four of the patients received definitive radiotherapy with a total dose of 60 Gy in 30 fractions. The PET imaging (see below) was performed prior to treatment and did not change the clinical management. Written informed consent was obtained from all patients and the study was approved by the regional committee for research ethics.

### PET/CT protocol

All examinations were performed after a minimum of six hours of fasting, using a Siemens Biograph 16 PET/CT-scanner (Biograph 16, Siemens, Erlangen, Germany). The PET image acquisition was initiated directly after intravenous injection of  $^{18}\text{F}$ FDG with a mean activity of 395 MBq (354–433 MBq). The D-PET series had a sampling time of 15 seconds the first three minutes, 30 seconds during the following eight minutes and two minutes for the remaining 34 minutes. The total scan time was 45 minutes. Images were reconstructed by OSEM iterative technique, with four iterations, eight subsets and a Gaussian smoothing filter with FWHM of 5.5 mm. The resulting PET matrix had

Table I. Patient cohort.

| Patient | Histology, grade                         | Tumor location  | Tumor volume (cm <sup>3</sup> ) | Treatment | Clinical status |
|---------|--|---|---------------------------------|-----------|-----------------|
| 1       | Leiomyosarcoma, III                      | Right thigh (Adductor)                                  | 126                             | S         | DOD             |
| 2       | Leiomyosarcoma, III                      | Near liver (Para portal)                                | 38                              | RT        | SD              |
| 3       | Pleomorphic undifferentiated sarcoma, IV | Left buttock (Posterior to gluteus maximus)             | 189                             | S         | DOD             |
| 4       | Liposarcoma, III                         | Near left knee joint (Proximal and medial)              | 311                             | S         | NED             |
| 5       | Pleomorphic undifferentiated sarcoma, IV | Left shoulder blade (Superior and posterior to scapula) | 408                             | RT        | DOD             |
| 6       | Leiomyosarcoma, IV                       | Left calf (Gastrocnemius)                               | 48                              | S         | NED             |
| 7       | Myxofibrosarcoma, IV                     | Right thigh (Proximal, anterior to femur)               | 231                             | S         | NED             |
| 8       | Leiomyosarcoma, III                      | Right hip (Inguinal)                                    | 56                              | S         | NED             |
| 9       | Schwannoma, III/IV                       | Right knee (Proximal and lateral to fibula)             | 511                             | RT        | DOD             |
| 10      | Leiomyosarcoma, III                      | Shoulder (Proximal and lateral to humerus)              | 252                             | RT        | SD              |
| 11      | Leiomyosarcoma, IV                       | Back (Posterior of angulus scapula)                     | 86                              | S         | NED             |

DOD, dead of disease; NED, no evidence of disease; RT, definitive radiotherapy; S, surgery and post-operative radiotherapy; SD, stable disease.

dimensions  $128 \times 128$ . The slice thicknesses were 2–4 mm. The corresponding CT image had 1.37 mm in-plane resolution stored as a  $512 \times 512$  matrix and 5 mm slice thickness. The glucose levels of the patients were in the range 5.1–6.8 mmol/L, which was deemed acceptable according to a 7 mmol/L exclusion criteria [14].

#### Pharmacokinetic analysis

The D-PET series were analyzed using custom made software in IDL 6.2 (ITT Visual Information Solutions, Boulder, USA). The temporal  $^{18}\text{F}$ FDG uptake patterns in all voxels were fitted to a two-compartment model and pharmacokinetic parameters were calculated. Compartmental models use interconnected pools of tracer to describe kinetics of an underlying process. The pools are mathematical constructs representing a particular form of the tracer with equivalent kinetics. The methodology is used in several settings and has been thoroughly described in the literature [15].

The particular model used in the current work makes some fundamental assumptions to reduce the complexity and enables us to capture the basic kinetics.  $^{18}\text{F}$ FDG is assumed to be evenly distributed in the blood with negligible concentration changes in the arterial – venous direction.  $^{18}\text{F}$ FDG binding to red blood cells and other proteins are assumed to be fast. Blood vessel size/permeability is assumed to be large, making  $^{18}\text{F}$ FDG transport into the tissue dependent on blood flow only. Cellular membrane transport is assumed fast and no distinction between interstitial and intracellular free (non-metabolized)  $^{18}\text{F}$ FDG is made.

Following Røe et al. [13],  $^{18}\text{F}$ FDG is assumed to be circulated by the blood until trapped within the cells during metabolism or filtered by the kidneys. The  $^{18}\text{F}$ FDG concentration in the blood, which reflects the availability of  $^{18}\text{F}$ FDG in the body, serves as the input into the model. This arterial input function (AIF, see below) was approximated from the whole blood  $^{18}\text{F}$ FDG concentration given in the D-PET images. Furthermore,  $^{18}\text{F}$ FDG is assumed to be transported from the blood into the tissue at a linear transfer rate  $K_1$  relative to the blood flow. This makes  $K_1$  a measure of capillary permeability and perfusion. Once in the tissue the non-metabolized  $^{18}\text{F}$ FDG is either metabolized at a linear relative rate  $k_3$ , or transported back into the bloodstream at a linear relative rate  $k_2$ . The metabolized compartment consists of intracellular  $^{18}\text{F}$ FDG irreversibly trapped after phosphorylation by hexokinase during glycolysis.

The sum of non-metabolized (free), metabolized (bound), and intravascular compartments was

fitted by least squares optimization (Levenberg–Marquardt) to the time activity sequence in each voxel, producing estimates of the pharmacokinetic transfer rates. In addition, it was assumed that a certain fraction  $v_p$  of each voxel contained blood vessels, which was estimated in the least squares optimization as a fraction of the AIF. In the least squares procedure a low pass filter, averaging the closest six neighboring voxels, was applied to the input data to reduce noise. Bootstrapping was used to estimate uncertainties in parameter estimates.

#### Arterial input function

The time development of the  $^{18}\text{F}$ FDG concentration in the blood plasma, used as input in the pharmacokinetic model, is called the arterial input function (AIF). It has been shown that the time-activity plasma functions can be obtained non-invasively from images with regions of interest (ROI) defined over large vascular structures like the aorta or left ventricle [16]. Although the best results are obtained from the thoracic aorta, sampling of femoral arteries may give adequate results [17]. In the present work an averaged signal from a ROI defined over the aorta or femoral arteries was fitted to a tri-exponential function. A population AIF from seven patients with well-defined AIFs was used for all patients. This was done to avoid effects of the limited spatial resolution on the smaller fibular arteries in the scans of the tumors in the calves.

#### Output parameters

The D-PET images were normalized to injected dose and patient weight, giving a standardized uptake value (SUV) [18]:

$$\text{SUV} = \frac{\text{radioactivity concentration [Bq/kg]} \times \text{body mass [kg]}}{\text{injected activity [Bq]}} \quad (1)$$

Two time points in the dynamic series were given special attention.  $\text{SUV}_L$  refers to the image sampled in the interval 41–45 minutes after injection and  $\text{SUV}_E$  refers to the image sampled 1.5–2.5 minutes after injection.  $\text{SUV}_E$  has been shown to be an estimate for perfusion, and represents an alternative to the pharmacokinetic model parameters [6].  $\text{SUV}_L$  basically reflects the image obtained from conventional, static PET.

$\text{MR}_{\text{FDG}}$  describes the amount of metabolized  $^{18}\text{F}$ FDG relative to the  $^{18}\text{F}$ FDG level in the blood, and is calculated according to [12]:

$$\text{MR}_{\text{FDG}} = \frac{K_1 \cdot k_3}{k_2 + k_3} \quad (2)$$

Peak values were extracted for all PET images and parametric images. The peak value was obtained by identifying the most intense voxel of the tumor, and calculating the mean intensity in a  $1\text{ cm}^3$  volume around this voxel [19].

### Statistics

Correlations (denoted  $r$ ) between different image parameters were calculated by Pearson's correlation coefficient. The quality of the tracer kinetic curve fit was quantified with the squared Pearson's correlation coefficient between the original data and the fitted curve ( $r^2$ ). Clinical factors included were tumor size, grade and clinical status. Correlations between image parameters and clinical factors were calculated by Spearman's correlation coefficient.

### Results

From visual inspections, the  $^{18}\text{F}$ FDG PET images obtained from the initial acquisition phase exhibited traits different from the final  $^{18}\text{F}$ FDG PET images in organs such as, e.g. the heart and lungs. This is clearly seen in the dynamic sequence for patient 11 (Figure 1). Here, during the first 0–2 min p.i., high

$^{18}\text{F}$ FDG uptake is primarily seen in the lung, heart and major arteries. During the next 2–10 minutes p.i. the activity in these regions decreases. In the time period 10–45 min p.i. the activity in the blood and normal tissue continues to decrease, while metabolically active regions such as the parts of the tumor show increased uptake. This development is also seen in the time-uptake curves in the tumors, where  $\text{SUV}_{\text{peak}}$  changes rapidly during the early acquisition phase (Figure 2). Thereafter, slower uptake is found, except for patients 5, 8 and 9, where the uptake curves show no sign of saturation during the acquisition time. Interestingly, four of the tumors (patients 2, 7, 10 and 11) show higher peak  $^{18}\text{F}$ FDG concentrations in the early acquisition phase compared to the late phase.

Figure 3 shows uptake curves in individual voxels for patient 1. Large intervoxel variations in the uptake curves are generally seen, and some intravoxel noise is also present. The tracer kinetic curve fitting gave  $r^2$  values (averaged over each tumor) ranging from 0.31–0.96. The variations in temporal uptake patterns are reflected in variations in the free/bound curve components and resulting tracer kinetic parameters. From the curve fitting, mean parameter estimates (over all patients and voxels) with

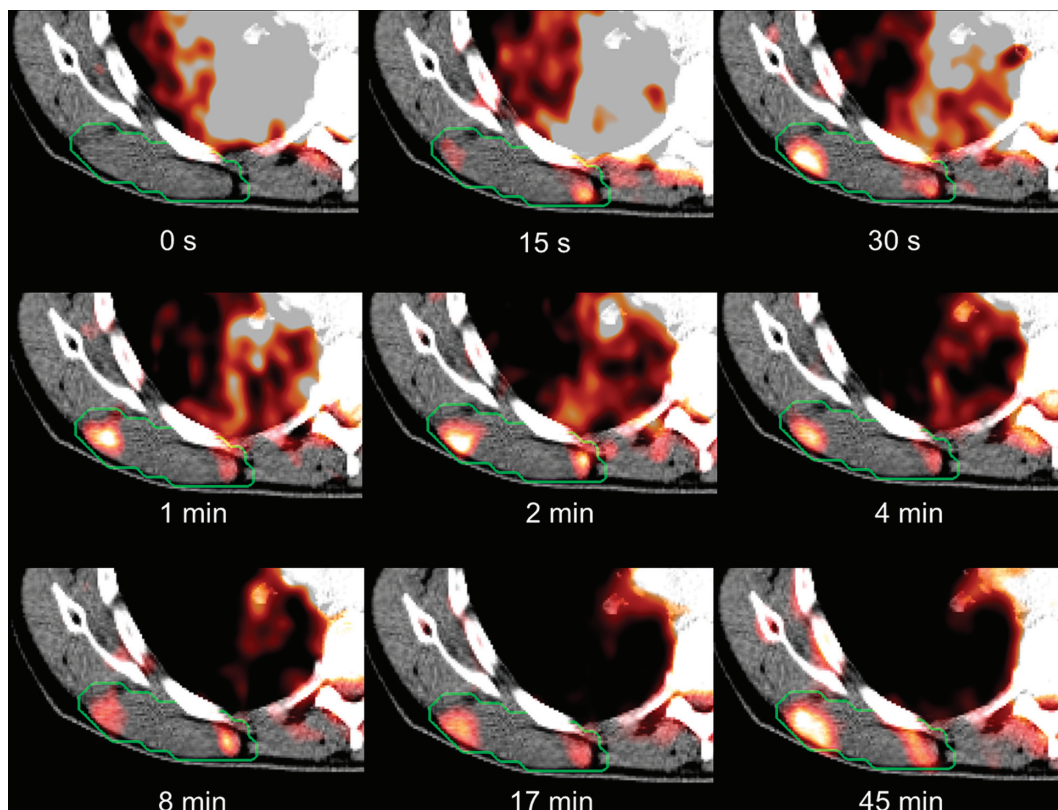


Figure 1. Dynamic  $^{18}\text{F}$ FDG-PET sequence for patient 11 post injection showing the temporal evolution of the FDG activity. The tumor border is marked with a green line.

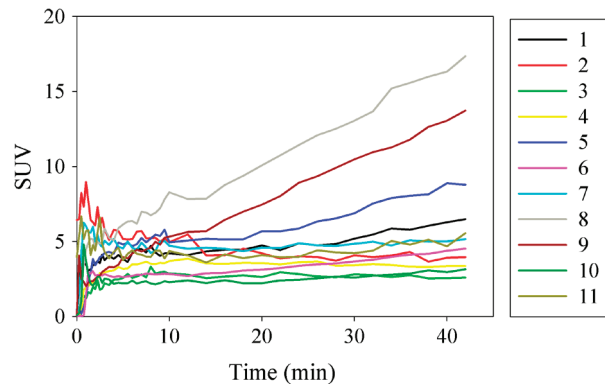


Figure 2. Time activity curves for patients 1-11 post injection showing the temporal development of the SUV peak value.

mean errors were  $K_1 = 0.20 \pm 0.062$ ,  $k_2 = 0.44 \pm 0.11$ ,  $k_3 = 0.028 \pm 0.007$ ,  $v_p = 0.048 \pm 0.011$ , and  $MR_{FDG} = 0.0015 \pm 0.0003$ .

The kinetic parameters show a systematic spatial pattern for most patients, with elevated intensity in the tumor compared to the surrounding normal tissues, as can be seen in patient 11 (Figure 4). The resulting parametric maps share many of the attributes of the static images.  $SUV_E$  is related to the

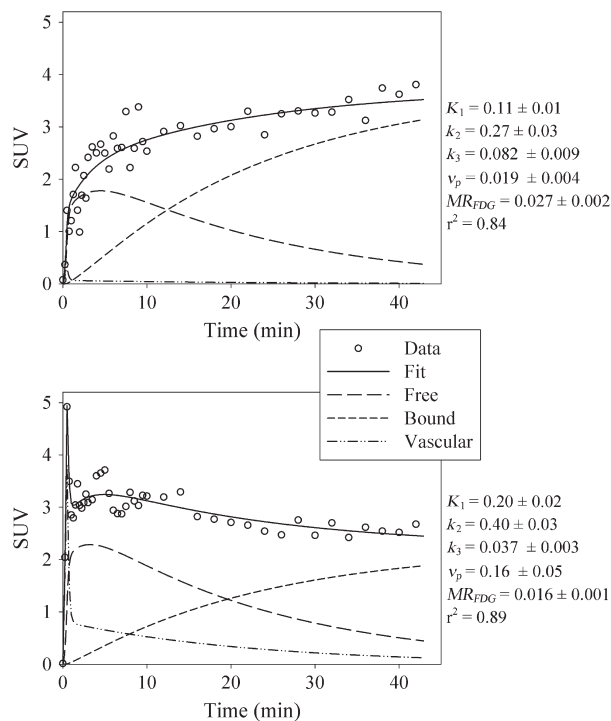


Figure 3. Two selected voxel elements for patient 10 post injection. Data points are averaged over the voxel in question and its six closest voxels. “Free” is non-metabolized  $^{18}\text{F}$ FDG, “bound” is metabolized  $^{18}\text{F}$ FDG, and “vascular” is the fraction of the plasma function included in the voxel element. Estimated pharmacokinetic parameters are given.

vascular parameters such as  $K_1$  and  $v_p$  while  $SUV_L$  is related to the metabolic parameters such as  $k_3$  and  $MR_{FDG}$ . Combining all patients, a cohort-based histogram of the parameter values was obtained (Figure 5). Most histograms appear to have a normal to log-normal distribution. Variations are seen, however, both in the center and in the width of the distributions.

Comparing the peak values of the image parameters reveal quite large variations between patients (Table II). Significant ( $p < 0.05$ ) correlations were found between the peak values of  $SUV_L$  and  $MR_{FDG}$  ( $r = 0.99$ ),  $SUV_E$  and  $v_p$  ( $r = 0.90$ ),  $SUV_E$  and  $K_1$  ( $r = 0.79$ ),  $K_1$  and  $v_p$  ( $r = 0.80$ ) and  $K_1$  and  $k_2$  ( $r = 0.74$ ).  $SUV_E$  and  $SUV_L$  were not correlated ( $r = 0.06$ ). No significant correlations were found between the PET values and clinical factors, although  $v_p$  was close to being significantly correlated with clinical status ( $r = 0.60$ ,  $p = 0.052$ ).

## Discussion

In the current work dynamic  $^{18}\text{F}$ FDG-PET and pharmacokinetic analysis in a selection of patients with soft tissue sarcomas has been described. It appears that complementary information may be obtained both from the early and the late uptake phase as the corresponding parameters ( $SUV_E$  and  $SUV_L$ ) were not correlated. The early phase is interesting for two reasons. First, it has the ability to describe aspects of the vasculature of the tissue. Second, the early phase has implications for the subsequent late phase which is used to describe metabolism.

Immediately after injection,  $^{18}\text{F}$ FDG is a concentrated bolus and the initial  $^{18}\text{F}$ FDG D-PET images thus visualize the major arteries, the heart and the lungs. In the first minutes after the bolus reaches the tumor the  $^{18}\text{F}$ FDG diffuses from the blood vessels into the interstitial space. In this period the tissue uptake is primarily determined by blood perfusion and vascular permeability. In the subsequent metabolic phase  $^{18}\text{F}$ FDG is gradually accumulated in metabolically active cells. The blood concentration decreases as the  $^{18}\text{F}$ FDG is bound in the cells and filtered from the blood in the kidneys. The amount of  $^{18}\text{F}$ FDG that is metabolized in a given region of tissue is a function of available  $^{18}\text{F}$ FDG, the density of cells, the expression of GLUT transporters, the glycolytic enzyme hexokinase, and in normal cells; the presence of oxygen [20]. The metabolic potential of the cells is also defined by their genetics. Nutrient availability can change rapidly due to blood flow changes, caused by vascular occlusion, and due to altered

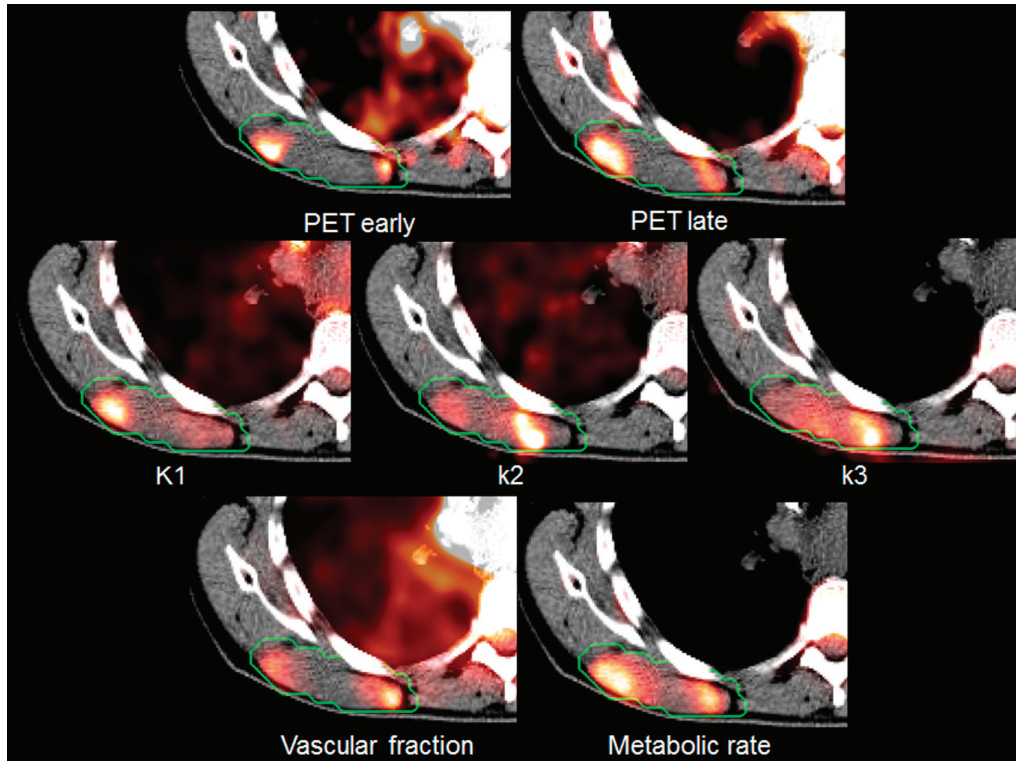


Figure 4. Parameter maps for patient 11 derived from the pharmacokinetic analysis. In addition, two static snapshot PET images obtained 2 and 45 min p.i. are shown. The tumor border is marked with a green line.

nutrient diffusion depths caused by tissue deformation during treatment.

Since the AIF is the basis of the pharmacokinetic analysis, errors in the function may have considerable impact on the result. This has previously been shown for pharmacokinetic analysis of DCE data [21]. Furthermore, red blood cells only process glucose for energy and the whole blood will inevitably include some metabolically bound FDG. The effect however is subtle, systemic, repeatable, and aside from differences in the hematocrit should be similar in all patients. Another source of error is internal and external patient motion, resulting in displaced plasma sample points in the D-PET images. This is particularly the case for sample points taken from arteries of comparable diameter as the sampling voxels. Furthermore, the actual plasma peak in the dynamic sequences is seldom seen as more than a point, probably due to the coarse sampling time of 15 seconds.

Studies have reported the ability of static  $^{18}\text{F}$ FDG PET to predict treatment outcome and progression of soft tissue sarcomas [2,3,22]. Other studies have shown similar abilities for DCE-MRI [23], and studies combining vascular and metabolic information have found improved predictions of patient survival [24,25]. However; to our knowledge no conclusive standardization of

parameter selection has been established. Very few studies of relevance to the current work have addressed pharmacokinetic curve analysis from  $^{18}\text{F}$ FDG D-PET of solid tumors. In a study comprising 31 soft tissue sarcoma patients,  $K_1$ ,  $k_3$  and  $v_p$  were about and  $0.5 \text{ min}^{-1}$ ,  $0.05 \text{ min}^{-1}$  and  $0.1$ , respectively (cohort-based median values) [7]. These estimates are quite in line with those found in the current work. Furthermore, a study on 75 patients with breast cancer gave  $K_1$  and  $\text{MR}_{\text{FDG}}$  values of about  $0.13 \text{ min}^{-1}$  and  $0.025 \text{ min}^{-1}$ , respectively, also comparable to the values found in the current work [26].

In this paper, three parameters were assumed to describe glucose metabolism:  $\text{SUV}_L$ ,  $\text{MR}_{\text{FDG}}$  and  $k_3$ .  $\text{SUV}_L$  is by far the most frequently used surrogate measure for hypermetabolism, as it represent the SUV obtained from static, conventional PET.  $\text{SUV}_L$  closely resembles  $\text{MR}_{\text{FDG}}$ , though the latter is less dependent on the vasculature. The pharmacokinetic parameter  $k_3$  describes the cellular expression of the glycolytic enzyme hexokinase and represents the metabolic potential of the cells. The time-SUV curves (Figure 2) reveal heterogeneity in temporal glucose distribution among the tumors. They also show that a distinct vascular phase does not necessarily imply a strong metabolic phase. A single static value acquired 45 min

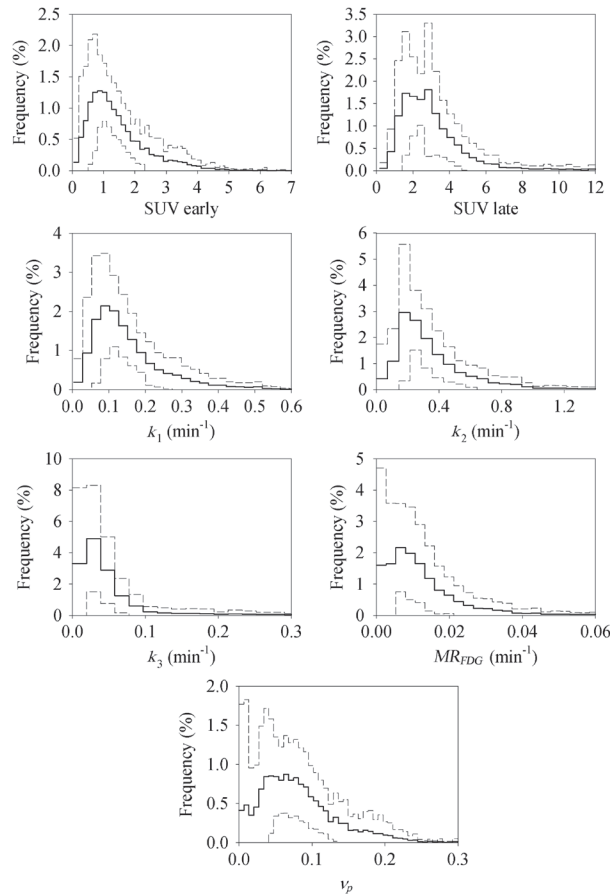


Figure 5. Patient-averaged histograms over the relevant PET-derived parameters. The dashed lines indicate one standard deviation.

p.i. ( $SUV_L$ ), as obtained from conventional PET, is therefore not descriptive for the vascular phase of  $^{18}\text{F}$ FDG distribution. Valuable information of tumor physiology may thus be lost in conventional, static PET.

The vascular parameter maps  $K_1$ ,  $k_2$ ,  $v_p$  and  $SUV_E$  describe different properties of the blood

supply. Still, the peak parameter values in the tumors correlate significantly with each other, and a simple static value some minutes after injection ( $SUV_E$ ) may be considered an alternative to a complete pharmacokinetic analysis. A short static image acquisition at the time of injection, providing  $SUV_E$  and letting the patient rest for 45 minutes prior to the next static acquisition (giving  $SUV_L$ ) could reduce the burden to the patient. However, this would necessitate an additional co-registration between the images obtained during the early and late acquisition. Furthermore, the peak values of the metabolic parameters  $SUV_L$  and  $MR_{FDG}$  showed significant correlations with each other. Yet, they displayed different intensities in regions dominated by vasculature (Figure 4). The  $k_3$  parameter, on the other hand, produces values that highlight not only metabolically active regions but also regions combining some degree of metabolism with poor vasculature.

One disadvantage of using quantification parameters like max, peak or median, are the loss of voxel value distribution (Figure 5). For the metabolic parameters, high values represent pathology, while for the vascular parameters, the relation is not evident. Regions with high vascular parameter values may represent angiogenesis and tumor progression while regions with low values may represent hypoxia and cellular stress. Thus it may be necessary to examine the full histogram rather than focus on single values [27].

In conclusion, D-PET represents a method to obtain both vascular and metabolic information in a single examination. In the present study, no predictive parameters for patient survival could be detected. However, sarcomas are a heterogeneous class of tumors and further clinical studies are required in order to get more insight into the role of dynamic PET scanning for management of these diseases.

Table II. Summary of PET-derived values.

| Patient | $SUV_E$ | $SUV_L$ | $K_1$ ( $\text{min}^{-1}$ ) | $k_2$ ( $\text{min}^{-1}$ ) | $k_3$ ( $\text{min}^{-1}$ ) | $MR_{FDG}$ ( $\text{min}^{-1}$ ) | $v_p$ |
|---------|---------|---------|-----------------------------|-----------------------------|-----------------------------|----------------------------------|-------|
| 1       | 3.3     | 5.9     | 0.31                        | 0.66                        | 0.087                       | 0.033                            | 0.15  |
| 2       | 6.0     | 4.3     | 0.54                        | 1.07                        | 0.032                       | 0.012                            | 0.27  |
| 3       | 1.5     | 2.5     | 0.19                        | 0.54                        | 0.032                       | 0.007                            | 0.07  |
| 4       | 2.1     | 3.3     | 0.20                        | 0.25                        | 0.017                       | 0.009                            | 0.14  |
| 5       | 3.0     | 8.1     | 0.39                        | 0.73                        | 0.16                        | 0.062                            | 0.18  |
| 6       | 2.9     | 4.4     | 0.27                        | 0.79                        | 0.088                       | 0.026                            | 0.12  |
| 7       | 5.8     | 5.0     | 0.59                        | 0.94                        | 0.056                       | 0.021                            | 0.27  |
| 8       | 4.4     | 16.3    | 0.61                        | 1.14                        | 0.283                       | 0.126                            | 0.25  |
| 9       | 2.8     | 13.1    | 0.27                        | 2.03                        | 0.95                        | 0.088                            | 0.11  |
| 10      | 3.7     | 3.0     | 0.19                        | 0.56                        | 0.071                       | 0.016                            | 0.20  |
| 11      | 5.4     | 4.7     | 0.97                        | 2.41                        | 0.174                       | 0.025                            | 0.20  |

$MR_{FDG}$ , metabolic rate of  $^{18}\text{F}$ FDG;  $SUV_E$ , peak standard uptake value 2 minutes post injection;  $SUV_L$ , peak standard uptake value 45 minutes post injection;  $v_p$ , vascular fraction.

## Acknowledgements

Dr. Trond Velde Bogsrud is gratefully acknowledged for contributing to the initiation of the project.

**Declaration of interest:** The authors report no conflicts of interest. The authors alone are responsible for the content and writing of the paper.

## References

- [1] Jebesen NL, Bruland OS, Eriksson M, Engellau J, Turesson I, Folin A, et al. Five-year results from a Scandinavian sarcoma group study (SSG XIII) of adjuvant chemotherapy combined with accelerated radiotherapy in high-risk soft tissue sarcoma of extremities and trunk wall. *Int J Radiat Oncol Biol Phys* 2011;81:1359–66.
- [2] Benz MR, Czernin J, Allen-Auerbach MS, Tap WD, Dry SM, Elashoff D, et al. FDG-PET/CT imaging predicts histopathologic treatment responses after the initial cycle of neoadjuvant chemotherapy in high-grade soft-tissue sarcomas. *Clin Cancer Res* 2009;15:2856–63.
- [3] Kasper B, Dietrich S, Dimitrakopoulou-Strauss A, Strauss LG, Haberkorn U, Ho AD, et al. Early prediction of therapy outcome in patients with high-risk soft tissue sarcoma using positron emission tomography. *Onkologie* 2008;31:107–12.
- [4] Fletcher JW, Djulbegovic B, Soares HP, Siegel BA, Lowe VJ, Lyman GH, et al. Recommendations on the use of  $^{18}\text{F}$ -FDG PET in oncology. *J Nucl Med* 2008;49:480–508.
- [5] Malinen E, Rodal J, Knudtsen IS, Sovik A, Skogmo HK. Spatiotemporal analysis of tumor uptake patterns in dynamic  $(^{18}\text{F})\text{FDG}$ -PET and dynamic contrast enhanced CT. *Acta Oncol* 2011;50:873–82.
- [6] Mullani NA, Herbst RS, O'Neil RG, Gould KL, Barron BJ, Abbruzzese JL. Tumor blood flow measured by PET dynamic imaging of first-pass  $^{18}\text{F}$ -FDG uptake: A comparison with  $^{15}\text{O}$ -labeled water-measured blood flow. *J Nucl Med* 2008;49:517–23.
- [7] Dimitrakopoulou-Strauss A, Strauss LG, Egerer G, Vasamiliette J, Schmitt T, Haberkorn U, et al. Prediction of chemotherapy outcome in patients with metastatic soft tissue sarcomas based on dynamic FDG PET (dPET) and a multiparameter analysis. *Eur J Nucl Med Mol Imaging* 2010;37:1481–9.
- [8] Raghunand N, Gatenby RA, Gillies RJ. Microenvironmental and cellular consequences of altered blood flow in tumours. *Br J Radiol* 2003;76:S11–22.
- [9] Aristophanous M, Yap JT, Killoran JH, Chen AB, Berbeco RI. Four-dimensional positron emission tomography: Implications for dose painting of high-uptake regions. *Int J Radiat Oncol Biol Phys* 2011;80:900–8.
- [10] Sovik A, Malinen E, Olsen DR. Strategies for biologic image-guided dose escalation: A review. *Int J Radiat Oncol Biol Phys* 2009;73:650–8.
- [11] Dimitrakopoulou-Strauss A, Strauss LG, Schwarzbach M, Burger C, Heichel T, Willeke F, et al. Dynamic PET  $^{18}\text{F}$ -FDG studies in patients with primary and recurrent soft-tissue sarcomas: Impact on diagnosis and correlation with grading. *J Nucl Med* 2001;42:713–20.
- [12] Phelps ME, Huang SC, Hoffman EJ, Selin C, Sokoloff L, Kuhl DE. Tomographic measurement of local cerebral glucose metabolic rate in humans with  $(\text{F}-18)2\text{-fluoro-2-deoxy-D-glucose}$ : Validation of method. *Ann Neurol* 1979;6:371–88.
- [13] Roe K, Aleksandersen TB, Kristian A, Nilsen LB, Seierstad T, Qu H, et al. Preclinical dynamic  $^{18}\text{F}$ -FDG PET – tumor characterization and radiotherapy response assessment by kinetic compartment analysis. *Acta Oncol* 2010;49:914–21.
- [14] Boellaard R, O'Doherty MJ, Weber WA, Mottaghy FM, Lonsdale MN, Stroobants SG, et al. FDG PET and PET/CT: EANM procedure guidelines for tumour PET imaging: Version 1.0. *Eur J Nucl Med Mol Imaging* 2010;37:181–200.
- [15] Phelps ME. PET: Molecular imaging and its biological applications. New York, NY: Springer-Verlag; 2004.
- [16] de Geus-Oei LF, Visser EP, Krabbe PF, van Hoorn BA, Koenders EB, Willemsen AT, et al. Comparison of image-derived and arterial input functions for estimating the rate of glucose metabolism in therapy-monitoring  $^{18}\text{F}$ -FDG PET studies. *J Nucl Med* 2006;47:945–9.
- [17] Puri T, Blake GM, Frost ML, Moore AE, Siddique M, Cook GJ, et al. Validation of image-derived arterial input functions at the femoral artery using  $^{18}\text{F}$ -fluoride positron emission tomography. *Nucl Med Commun* 2011;32:808–17.
- [18] Zasadny KR, Wahl RL. Standardized uptake values of normal tissues at PET with 2-[fluorine-18]-fluoro-2-deoxy-D-glucose: Variations with body weight and a method for correction. *Radiology* 1993;189:847–50.
- [19] Wahl RL, Jacene H, Kasamon Y, Lodge MA. From RECIST to PERCIST: Evolving considerations for PET response criteria in solid tumors. *J Nucl Med* 2009;50:122S–50S.
- [20] Bos R, van Der Hoeven JJ, van Der Wall E, van Der Groep P, van Diest PJ, Comans EF, et al. Biologic correlates of  $(^{18}\text{F})\text{fluorodeoxyglucose}$  uptake in human breast cancer measured by positron emission tomography. *J Clin Oncol* 2002;20:379–87.
- [21] Port RE, Knopp MV, Brix G. Dynamic contrast-enhanced MRI using Gd-DTPA: Interindividual variability of the arterial input function and consequences for the assessment of kinetics in tumors. *Magn Reson Med* 2001;45:1030–8.
- [22] Charest M, Hickeson M, Lisbona R, Novales-Diaz JA, Derbekyan V, Turcotte RE. FDG PET/CT imaging in primary osseous and soft tissue sarcomas: A retrospective review of 212 cases. *Eur J Nucl Med Mol Imaging* 2009;36:1944–51.
- [23] Alic L, van Vliet M, van Dijke CF, Eggermont AM, Veenland JF, Niessen WJ. Heterogeneity in DCE-MRI parametric maps: A biomarker for treatment response? *Phys Med Biol* 2011;56:1601–16.
- [24] Tseng J, Dunnwald LK, Schubert EK, Link JM, Minoshima S, Muzi M, et al.  $^{18}\text{F}$ -FDG kinetics in locally advanced breast cancer: Correlation with tumor blood flow and changes in response to neoadjuvant chemotherapy. *J Nucl Med* 2004;45:1829–37.
- [25] Dimitrakopoulou-Strauss A, Strauss LG, Egerer G, Vasamiliette J, Mechttersheimer G, Schmitt T, et al. Impact of dynamic  $(^{18}\text{F})\text{FDG}$  PET on the early prediction of therapy outcome in patients with high-risk soft-tissue sarcomas after neoadjuvant chemotherapy: A feasibility study. *J Nucl Med* 2010;51:551–8.
- [26] Dunnwald LK, Doot RK, Specht JM, Gralow JR, Ellis GK, Livingston RB, et al. PET tumor metabolism in locally advanced breast cancer patients undergoing neoadjuvant chemotherapy: Value of static versus kinetic measures of fluorodeoxyglucose uptake. *Clin Cancer Res* 2011;17:2400–9.
- [27] Andersen EK, Hole KH, Lund KV, Sundfor K, Kristensen GB, Lyng H, et al. Dynamic contrast-enhanced MRI of cervical cancers: Temporal percentile screening of contrast enhancement identifies parameters for prediction of chemoradioresistance. *Int J Radiat Oncol Biol Phys* 2012;82:e485–92.